

Strain Mapping at the Atomic Scale in Highly Mismatched Heterointerfaces**

By Ana María Sánchez,* Juan Gabriel Lozano, Rafael García, Miriam Herrera, Sandra Ruffenach, Olivier Briot, and David González

A complete characterization of dislocation network in a highly mismatched interface with high spatial resolution has been performed. The interface between InN quantum dots and a (0001) GaN substrate contains three noninteracting sets of regularly-spaced misfit dislocations lying along $\langle 11\bar{2}0 \rangle$ directions. The network has a “Star of David” form, with each star bounding a hexagonal region which is pseudomorphic. These misfit dislocations form a threading dislocation network at the island edges due to free surface forces.

1. Introduction

Growth of nanostructures on substrates with large lattice mismatch is unavoidable for many technological applications. The different lattice parameters of the materials gives rise to a misfit strain, $f = (a_l - a_s)/a_s$, in the layer, where a_l and a_s are the lattice parameters of layer and substrate respectively, which gradually decreases through the generation of crystalline defects. Relaxation process such as the generation of dislocations, stacking faults, cracks and tilts are observed. The formation of a misfit dislocation array at the interface reduces the total free energy in the system, but can also result in deterioration in the functional properties of the structure. Thus, the knowledge of the misfit dislocation network can be important in heteroepitaxial design and technology, since the development and fabrication of devices is restricted by the structural defects associated with the growth of epilayers on different substrates.

In low mismatch systems, the models of Frank and Van Der Merwe,^[1] and of Matthews and Blakeslee,^[2] based on thermodynamic equilibrium, are often used. At a critical thickness h_c

activation of slip system occurs and the strained (pseudomorphic) film begins to relax. Generally, the dislocation misfit network in these low mismatch systems are easily observed using conventional transmission electron microscopy (CTEM). However, these critical thickness models are not appropriate for many heteroepitaxial systems which have a large lattice mismatch ($f > 4\text{--}5\%$), such as GaN/Al₂O₃, V/Al₂O₃, GaN/Si(111), SiC/Si, or InN/GaN. In these cases, the critical thickness becomes less than one monolayer so a geometrical misfit dislocation network accommodates the most of the mismatch in these systems. These misfit dislocations arise from a different mechanism in comparison with the classical Van Der Merwe–Matthews type.^[3] Since pseudomorphic growth of highly mismatched structures is close to impossible, extra-half planes in the epilayer or substrate define the geometrical misfit dislocations from the very beginning of epitaxial growth.^[4] The final configuration for both low and highly mismatched interfaces consists of coherent regions separated by misfit dislocations.

In general, periodic arrays of misfit dislocations are not easily observed at largely mismatched interfaces, unlike well-known structures such as SiGe/Si and InGaAs/GaAs, since the dislocations are too closely spaced to be resolved. Cross-sectional high resolution TEM (HRTEM) is the main technique commonly used to estimate the misfit dislocation density in highly mismatched systems. The edge component of a misfit dislocation is seen as an extra half-plane in the material with smaller lattice parameter, providing an estimate of the spacing between the misfit dislocations, i.e., linear dislocation density. In addition, a Burgers circuit drawn around the area containing the half-planes gives information about the sign and magnitude of the edge component of the corresponding Burgers vectors. However, this is an incomplete description. Many relevant features such as changes in line direction and/or interaction with other misfit dislocations cannot be determined. More information is obtained when the dislocation array is observed in a planar orientation, where the interfacial plane is parallel to the surfaces of the thin specimen. Cross section HRTEM is only used for highly misfit systems because the dislocation image

[*] Dr. A. M. Sánchez, J. G. Lozano, Prof. R. García, Dr. D. González
Departamento de Ciencia de los Materiales e Ingeniería Metalúrgica
y Química Inorgánica, Universidad de Cádiz
Apdo. 40, 11510 Puerto Real (Cádiz) (Spain)
E-mail: ana.fuentes@uca.es

Dr. M. Herrera
Department of Chemical Engineering and Materials Science
University of California Davis
One Shields Ave, Davis, 95616 CA (USA)

Dr. S. Ruffenach, Dr. O. Briot
Groupe d'Etudes des Semiconducteurs, Université Montpellier II
UMR 5650 CNRS
Place Eugène Bataillon, 34095 Montpellier, (France)

[**] The authors are grateful to Dr. Pedro Galindo and Dr. Richard Bealand for interesting and fruitful discussions. Financial support from CICYT project MAT2004-1234 (Spain) and SANDIE European Network of Excellence (NMP4-CT-2004-500101—Sixth Framework Program) is gratefully acknowledged.

width in conventional planar view diffraction contrast techniques is close to, or larger than, the dislocation spacing, with the result that individual dislocations cannot be resolved.

In recent years, the analysis of high resolution TEM images using peak finding^[5,8,9] (PF) and/or geometric phase^[6–8] (GP) methodologies has become more widely practised. This allows quantitative strain mapping at very high spatial resolution in crystalline materials^[8–10] using high resolution transmission electron microscopy (HRTEM) images. The aim of this article is to demonstrate that HRTEM images of planar view specimens allow a complete characterisation of the misfit dislocation network in highly mismatched interfaces. We have applied this technique to InN/GaN quantum dots. We will demonstrate that the misfit dislocations in this system lie along $\langle 11\bar{2}0 \rangle$ directions, creating a hexagonal network. These misfit dislocations do not interact, and there is no evidence of dislocation node formation. In addition, this analysis has also revealed threading dislocation networks around the QD, demonstrating the tendency of edge misfit dislocations in highly misfit systems to bend towards the free surface, producing an edge-threading network.

2. Results and Discussion

Figure 1a shows the moiré fringe pattern in an area containing an InN quantum dot in InN/GaN heterostructure. Moiré fringe patterns are ubiquitous in planar view micrographs of highly mismatched systems. These patterns arise from the interference between electron beams diffracted from two overlapping materials with different lattice parameters. The left-top inset shows the corresponding digital diffractogram using a fast Fourier transform (FFT). The diffractogram shows the InN orientation is $\langle 0001 \rangle$, consistent with the GaN(0001) buffer layer. This also shows that here is essentially zero rotation between the $\{1\bar{1}00\}$ directions in the InN island and the GaN substrate. Therefore, the moiré fringes pattern is of the translational type, arising solely from the different lattice parameters of the two materials ($a_{\text{GaN}} = 0.3189$ nm and $a_{\text{InN}} = 0.3533$ nm). The left-bottom inset in Figure 1a is a magnified image showing the moiré fringes in more detail, where the sharp and blurred contrast of the atomic column projections correspond to good and bad fit between the InN/GaN lattices.

A Wiener filter was performed on Figure 1a, which estimates the noise locally

in the FFT image and—for each spatial frequency—the amplitude of the FFT, reducing the noise in the image. A Bragg filter was applied to the FFT, taking the Bragg peaks corresponding to the GaN and InN and neglecting double diffraction peaks. Double diffraction leads to the formation of the moiré fringes. In the filtered image, we have avoided the doubly diffracted beams and thus the filtered image using Bragg filter taking the GaN and InN Bragg peaks does not contain information about the moiré fringes. The Bragg masks applied in the diffractogram had a radius of 0.256 nm⁻¹. Six sets of symmetric Gaussian masks were placed around the $\{1\bar{1}00\}$ reflections (which included both the GaN and InN), allowing to remove the contribution of the double diffraction, but big enough to keep the fine details and do not remove any information from the InN, and GaN Bragg peaks. The phase images were obtained applying Gaussian masks around $\{1\bar{1}00\}$ Bragg peaks.

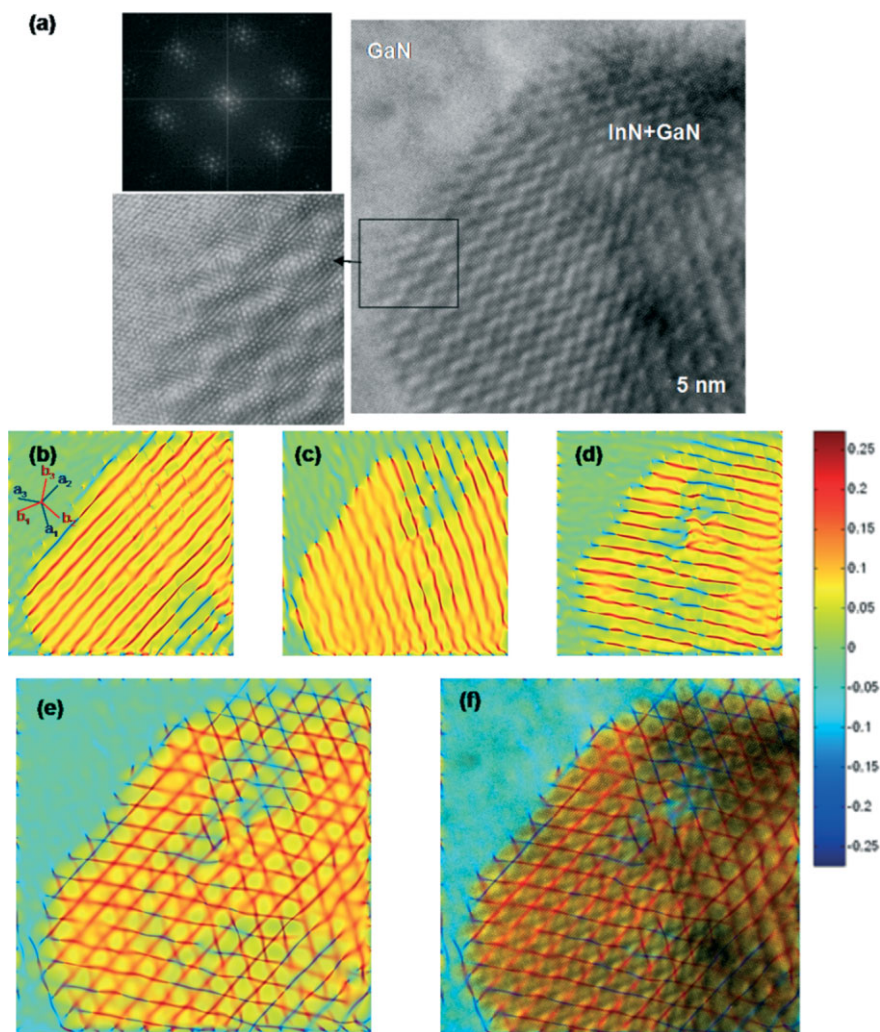


Figure 1. a) Plan-view HRTEM image along the $[0001]$ axis of InN/GaN. The top-left inset corresponds to the diffractogram and the bottom-left to a magnified region to demonstrate the resolved moiré fringes. b)–d) visualization of the three families of 60° misfit dislocation in the heterostructure. In the reference system the \mathbf{b} directions lie parallel the $\langle 1\bar{1}00 \rangle$ directions and the \mathbf{a} directions would correspond to the $\langle 11\bar{2}0 \rangle$ directions. e) combined image (b)–(d), and f) HTREM images superimposed with the misfit dislocation network.

The GP algorithm is based on the calculation of the displacement field and subsequently the strain map by numerical derivatives, from the phase images for different and non-collinear vectors. A full description of the methodology can be found in reference.^[7,9] GaN away from the InN quantum dot was chosen as reference material. By combining the phase images, the displacement can be calculated and subsequently the strain field by numerical differentiation using:^[6,11]

$$u(r) = -\frac{1}{2\pi} [P_{g1}(r)a_1 + P_{g2}(r)a_2] \quad (1)$$

$$\varepsilon_{ij} = \frac{1}{2} \left(\frac{\partial u_i}{\partial x_j} + \frac{\partial u_j}{\partial x_i} \right) \quad (2)$$

where P_g is the phase image and a_i and g_i the real space and reciprocal lattice vectors respectively.

The image processing and calculation of the strain field were performed using routines written in Matlab. The scale corresponds to the relative strain, ε' with zero corresponding to the GaN buffer without the InN quantum dot and defined as:

$$\varepsilon' = \frac{a - a_{GaN}^0}{a_{GaN}^0} \quad (3)$$

where a is the experimentally measured lattice parameter, and the superscript 0 correspond to unstressed crystal. The distortion field determined in this article is therefore calculated using the GaN as a reference, what is slightly different from the absolute strain:

$$\varepsilon_{InN} = \left| \frac{a_{InN}^{OD} - a_{InN}^0}{a_{InN}^0} \right| \propto \frac{a_{InN}^{OD} - a_{GaN}^0}{a_{GaN}^0} = \varepsilon' \quad (4)$$

From this expression we can conclude that the positive values indicate parameter $a_{InN}^0 < a_{InN}^{OD} < a_{GaN}^0$, i.e., a compressive distortion of the InN in areas corresponding to the quantum dot.

Figure 1b–d show the deformation maps corresponding to the three different sets of misfit dislocation in the InN/GaN system. The three sets of misfit dislocations are rotated with respect to each other by 60°. Figure 1e, obtained by combining Figure 1b–d, provides a very clear visualization of the misfit dislocation network, which accommodates the lattice misfit between the InN and GaN, and is in good agreement with previous reports.^[12] The average spacing between the dislocations is (2.70 ± 0.07) nm, giving a linear interfacial dislocation density, defined as the inverse of the average dislocation spacing, of $(3.7 \pm 0.1) \times 10^8$ cm⁻¹ along all three $\langle 1\bar{1}00 \rangle$ directions. This symmetry in the dislocation distribution indicates that geometrical misfit dislocations nucleate along the close packed $\langle 11\bar{2}0 \rangle$ directions. This reflects the 6-fold point symmetry of the two crystals in the same way as the pronounced difference in the linear interface dislocation densities along the two $\langle 110 \rangle$ directions in InGaAs/GaAs is consistent with the 2-fold point symmetry of that system.

In the InN/GaN system, the reciprocal lattice vectors $g = 1\bar{1}00$ are perpendicular to the direction of the dislocation lines. Figure 1a shows alternating regions corresponding to areas of good and bad fit between the two lattices. Sharp contrast corresponding to the atomic columns can be observed in the good fit regions. The superposition of the 60° misfit dislocation network with the HRTEM image is shown in Figure 1f. The misfit dislocations lie in areas corresponding to bad fit between the two crystals. The strain map shows a regular distribution of hexagonal regions with a pseudomorphic growth separated by a misfit dislocation network with the six-fold symmetry of the (0001) plane. As can be clearly observed in Figure 1e and f these misfit dislocations do not interact between themselves, so no dislocation nodes are created in the hexagonal network junctions. Therefore, the misfit dislocation network at the InN/GaN interface forms a David's star distribution instead of a hexagonal honeycomb observed in similar systems.^[13,14] Sharp atomic column contrast, indicating a good fit between the InN and substrate, is clearly observed in both the hexagonal and triangular areas. These images show that the InN QDs develop hexagonal areas with atomic columns perfectly adjusted with the GaN substrate without threading dislocations.^[15] The area of these hexagons is ~ 4.7 nm² resulting in a 70% at the whole interface free of strain.

As we can see in the Figure 1, blue lines inside the quantum dot that would indicate areas under a very tensile strain exist. They correspond to artefacts from the geometric phase methodology that does certainly not correspond to a real situation in the QD areas. The large dimensions of this image imply the existence of some areas, where the noise affects the image quality for quantitative analysis. On high-resolution images, the most important noise is due to the thin foil irregularities, which is almost unavoidable. These irregularities could also give rise to contrast errors, and the quantitative analysis fails in these areas.

To complete this misfit dislocation study at the highly mismatched interface, a discussion of the threading dislocation segments is required. The geometric phase analysis also provides information about the misfit dislocation behaviour close to the edge of the InN QD. Information on the state of the stress field can be obtained from the measured distortion from HRTEM images. Stress components were calculated, based on the elastic theory approach,^[16] from the deformation mapping and corresponding elastic constants.^[17] The σ_{xx} , σ_{yy} , and σ_{xy} component of the stress fields obtained from the experimental measurements are gathered in Figure 2 (a–c, respectively). These stress components are in good agreement with the stress distribution around an edge threading dislocation.^[16] We thus interpret these images as showing a network of threading dislocations surrounding the InN QDs with edge orientation. These threading dislocations have a Burgers vector $b = 1/3\langle 1\bar{2}10 \rangle$, indicated by a white arrow in Figure 2a. However this experimental stress calculation has been obtained from a thin TEM section, so to quantify the real state of the stress in the system a more complex process than the elastic theory approach should be used, using the nonlinear modelling starting from the experimental deformation measurements.^[17,18]

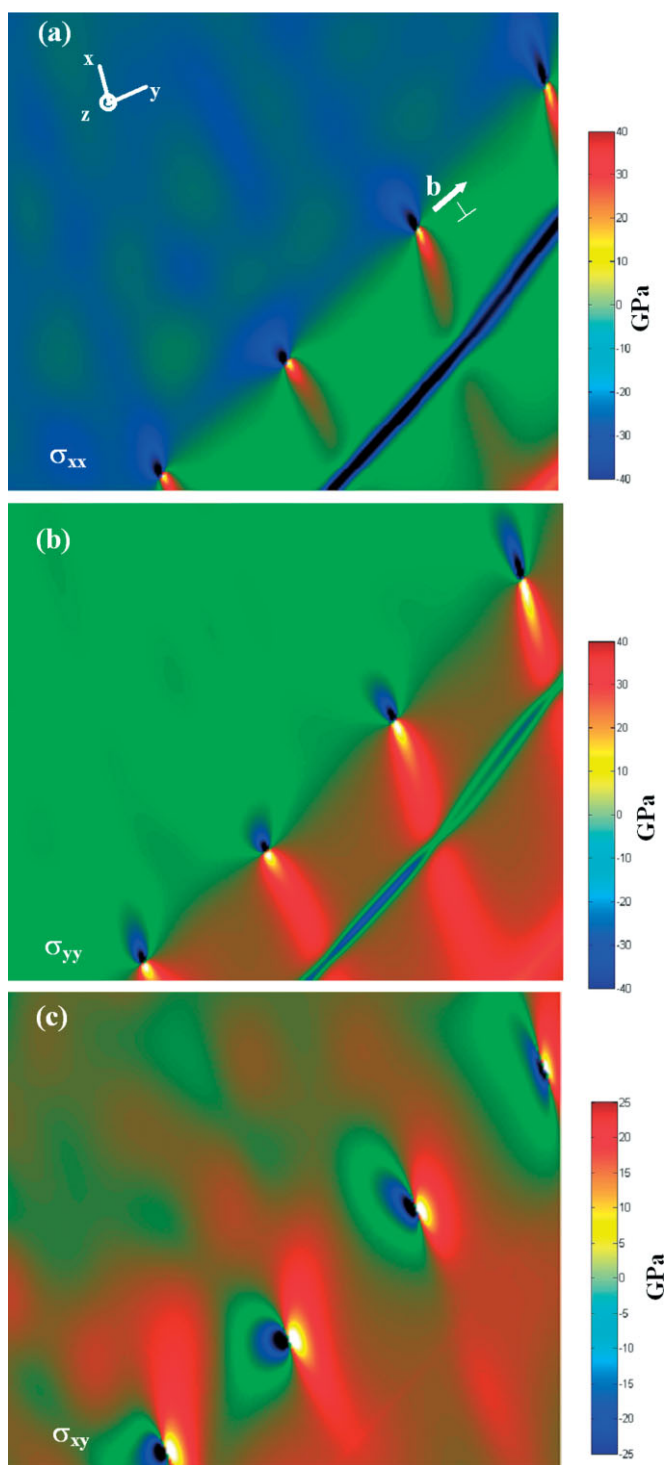


Figure 2. a) σ_{xx} , b) σ_{yy} , and c) σ_{xy} stress field component of the threading dislocation network. These distributions correspond to typical edge dislocations. The x and y directions correspond to $\langle 1\bar{1}00 \rangle$ and $\langle 11\bar{2}0 \rangle$ respectively being the dislocation vector \mathbf{b} parallel to the latter

This threading dislocation network around the InN QD was confirmed by conventional TEM. Figure 3a and b correspond to bright field and weak beam PVTEM images recorded under two beam conditions for $\mathbf{g} = 11\bar{2}0$ near the $\langle 0001 \rangle$ zone axis. In

Figure 3b, a threading dislocation arrangement surrounding the InN QDs is clearly visible. From the diffraction contrast invisibility criterion, these dislocations may possess Burgers vectors of $\mathbf{b} = 1/3\langle \bar{1}2\bar{1}0 \rangle$ or $\mathbf{b} = 1/3\langle \bar{1}2\bar{1}3 \rangle$, consistent with the results obtained by analysis of the HRTEM images. It has been previously reported that the mosaic structure in GaN is associated with the threading dislocation distribution at low angle boundaries,^[3] but these results demonstrate a tendency of the misfit dislocations to bend and form edge threading dislocations due to the influence of the free surface.

The slip system $1/3\langle \bar{1}2\bar{1}0 \rangle\{0001\}$ in this InN/GaN wurtzite heterostructure, with the basal plane parallel to the interface, is the main source of geometrical misfit dislocations. When these dislocations are close to the InN QD edge, they are attracted towards the free surface reducing the dislocation energy,^[19] giving rise to a threading dislocation network surrounding the QD, as we have demonstrated above. The slip systems which are possible for these threading dislocations, given that the Burgers vector lies along $\langle \bar{1}2\bar{1}0 \rangle$, are shown schematically in Figure 4. Those planes $(\bar{1}010)$, $(\bar{1}011)$ and $(\bar{1}012)$ are operative since the driving force acting on such slip planes is due to the nearness of the surface. This force decreases slowly with increasing distance from the surface, so in areas close to the interface the force induced by the surface is considerably stronger. Figure 4 shows three possible behaviours for a misfit dislocation running along the direction $\xi_{MD} = [2\bar{1}\bar{1}0]$ with a Burgers vector $\mathbf{b} = 1/3[\bar{1}2\bar{1}0]$. ξ_{TD} denotes the line direction for the threading segment and \mathbf{p} the slip plane. The small Peierls force acting on the dislocation is expected in the $1/3\langle \bar{1}2\bar{1}0 \rangle\{\bar{1}010\}$ slip system, since it presents the highest d/b ratio, which would give a line direction of $[0001]$. This is in good agreement with calculations using energetic considerations carried out by Mathis et al.^[20]

The observations of (a) a 60° misfit dislocation network at the high-misfit InN/GaN interface and (b) the threading dislocation network surrounding the InN QD, suggest the mechanism shown schematically in Figure 5. The InN QDs have a well-defined flat truncated hexagonal pyramidal shape in the uncapped heterostructure.^[21] A misfit dislocation running along $\langle \bar{1}2\bar{1}0 \rangle$ at the InN/GaN interface with a Burgers vector $\mathbf{b} = 1/3\langle 11\bar{2}0 \rangle$ interface has been depicted. When this misfit dislocation is close to the edge of the quantum dot, it is attracted towards the free surface and the dislocation bends along $[0001]$ in the $(10\bar{1}0)$ prismatic plane.

Further studies are required in order to understand this short TDs network behaviour. It would be attractive to analyse the coalescence between two islands to clarify the TDs movement along the boundary as well as the origin of the high TDs density observed in InN thick layers.^[22] In addition, the influence of the sample thickness in the strain mapping must be analysed. The measured distortions are probably different from a bulk sample due to the reduction of the substrate thickness. Since thin sections of investigated materials are constantly associated to the analysis carried out, these effects have to be taken into account in order to provide an accurate measurement of the distortion field. However, we consider that this fact does not affect the dislocation network distribution that highlight the

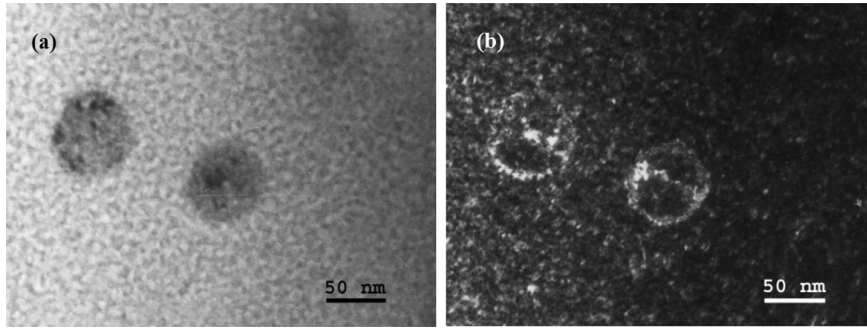


Figure 3. TEM planar view images of the sample: a) Bright field and b) weak beam showing the threading dislocations with an a-component Burgers vector around the InN QDs.

InN/GaN system. The misfit dislocations with $b = 1/3\langle 11\bar{2}0 \rangle$ hardly slip in the basal plane (0001) in hcp. structures, providing its characteristic brittle behaviour. Further analysis taking into account these factors is running at the moment, to get a more realistic and accurate distortion map of the highly mismatched systems.

3. Conclusions

We have demonstrated a complete description of the misfit dislocation network at a high-misfit interfaces using quantitative HRTEM of a planar view specimen. The dislocations are of 60° type and are almost symmetrically distributed inside the dot along the three $\langle 1\bar{2}\bar{1}0 \rangle$ directions at the interface, without any preferential one. A regular distribution of hexagonal regions with a pseudomorphic interface separated by a misfit dislocation network was revealed by strain mapping at atomic

scale. The interfacial dislocation network has a David's star form, consistent with the sixfold symmetry of the (0001) plane. Next to the QD edge, the dislocations bend up due to free surface forces, operating on the slip systems $1/3\langle 11\bar{2}0 \rangle(10\bar{1}0)$, which possess the smallest Peierls force. This mechanism has been confirmed by conventional TEM and also applying the GP algorithm to this threading dislocation segment to determine their stress field. Both are in good agreement with the theoretical stress field for edge threading dislocations.

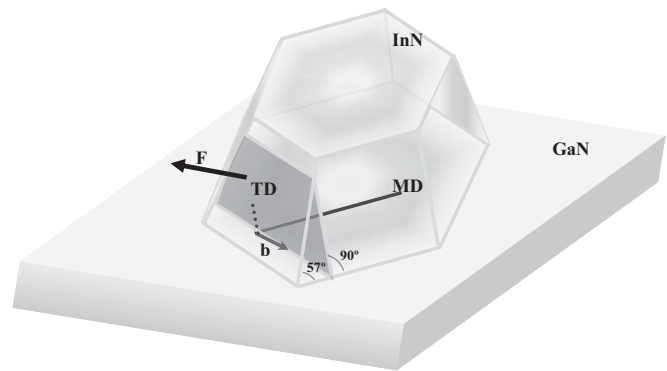


Figure 5. Proposed mechanism for the bending of the interfacial misfit dislocation network into threading segments.

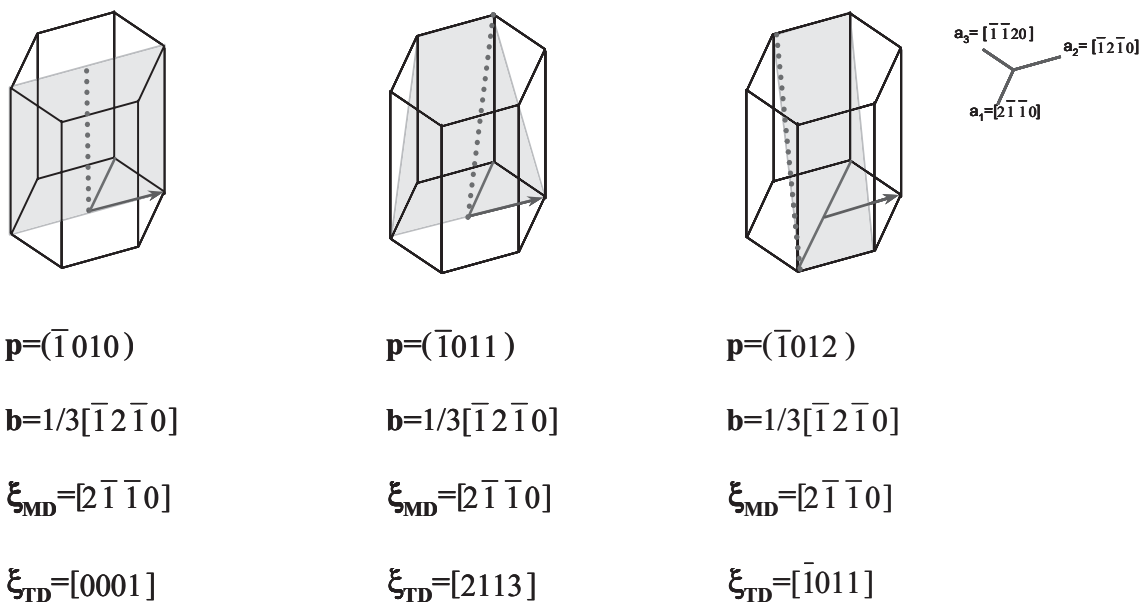


Figure 4. Schematic of the slip systems in wurtzite structure. a) $1/3\langle 1\bar{2}\bar{1}0 \rangle(\bar{1}010)$, b) $1/3\langle 1\bar{2}\bar{1}0 \rangle(\bar{1}011)$, and c) $1/3\langle 1\bar{2}\bar{1}0 \rangle(\bar{1}012)$. p indicates the plane, b the Burgers vector and the misfit and threading dislocation lines direction are ξ_{MD} and ξ_{TD} , respectively.

4. Experimental

InN quantum dots on GaN were chosen as a model system to determine the viability of the GP algorithm as a tool to study the misfit dislocation network in highly misfit interfaces. InN QDs were grown on GaN/Al₂O₃ by Metalorganic Vapour Phase Epitaxy. First, a buffer layer of GaN was grown using the classical two-step process on (0001) sapphire at a temperature close to 1000 °C. InN QDs were then deposited in the same growth run at a temperature of 550 °C, under a V/III molar ratio of 15 000, using ammonia (NH₃) as nitrogen precursor. Planar view specimen were prepared by mechanical grinding and dimpling to 10 µm, followed by ion milling to electron transparency. HRTEM observations were carried out in a JEOL 2011 at 200 kV.

Received: September 6, 2006

Revised: January 8, 2007

Published online: August 15, 2007

-
- [1] F. C. F. van der Merwe, *Proc. R. Soc. London Ser. A* **1949**, *198*, 216.
- [2] J. W. Matthews, A. E. Blakeslee, S. Mader, *Thin Solid Films* **1976**, *33*, 253.
- [3] X. J. Ning, F. R. Chien, P. Pirouz, J. W. Yang, M. A. Khan, *J. Mater. Res.* **1996**, *11*, 580.
- [4] V. Lebedev, W. Richter, in *Vacuum Science and Technology: Nitrides as seen by the Technology* (Eds: T. Paskova, B. Monemar), Research Signpost, Kerala, India **2002**.
- [5] R. Bierwolf, M. Hohenstein, F. Phillipp, O. Brandt, G. E. Crook, K. Ploog, *Ultramicroscopy* **1993**, *49*, 273.
- [6] M. J. Hÿtch, E. Snoeck, R. Kilaas, *Ultramicroscopy* **1998**, *74*, 131.
- [7] M. J. Hÿtch, T. Plamann, *Ultramicroscopy* **2001**, *87*, 199.
- [8] A. Rosenauer, T. Remmele, D. Gerthsen, K. Tillmann, A. Förster, *Optik* **1997**, *105*, 99.
- [9] S. Kret, P. Ruterana, A. Rosenauer, D. Gerthsen, *Phys. Status Solidi B* **2001**, *227*, 247.
- [10] P. Ruterana, S. Kret, A. Vivet, G. Maciejewski, P. Dłuzewski, *Appl. Phys. Lett.* **2002**, *91*, 8979.
- [11] J. L. Taraci, M. J. Hÿtch, T. Clement, P. Peralta, M. R. McCartney, J. Drucker, S. T. Picraux, *Nanotechnology* **2005**, *16*, 2365.
- [12] T. Tehagias, A. Delimitis, P. Komninou, E. Iliopoulos, E. Dimakis, A. Georgakilas, G. Nouet, *Appl. Phys. Lett.* **2005**, *86*, 151 905.
- [13] L. A. Zepeda-Ruiz, D. Maroudas, W. H. Weinberg, *Surf. Sci.* **1998**, *418*, L68.
- [14] H. Yamaguchi, J. G. Belk, X. M. Zhang, J. L. Sudijono, M. R. Fahy, T. S. Jones, D. W. Pashley, B. A. Joyce, *Phys. Rev. B* **1997**, *15*, 1337.
- [15] J. G. Lozano, A. M. Sánchez, R. García, D. Araújo, S. Ruffenach, O. Briot, D. González, *Appl. Phys. Lett.* **2005**, *87*, 263 104.
- [16] J. P. Hirth, J. Lothe, *Theory of Dislocations*, Wiley, New York **1982**.
- [17] S. P. Lepkowski, J. A. Majewski, G. Jurczak, *Phys. Rev. B* **2005**, *72*, 245201.
- [18] S. Kret, P. Dłuzewski, G. Maciejewski, V. Potin, J. Chen, P. Ruterana, G. Nouet, *Diamond Relat. Mater.* **2002**, *11*, 910.
- [19] D. Hull, D. J. Bacon, *Introduction to Dislocations*, Pergamon, Oxford **1984**.
- [20] S. K. Mathis, A. E. Romanov, L. F. Chen, G. E. Beltz, W. Pompe, J. S. Speck, *J. Cryst. Growth* **2001**, *231*, 371.
- [21] J. G. Lozano, D. González, A. M. Sánchez, D. Araújo, S. Ruffenach, O. Briot, R. García, *Phys. Status Solidi C* **2006**, *3*, 1687.
- [22] V. Lebedev, V. Cimalla, J. Pezoldt, M. Himmerlich, S. Krischok, J. A. Schaefer, O. Ambacher, F. M. Morales, J. G. Lozano, D. González, *J. Appl. Phys.* **2006**, *100*, 094 902.
-